J|A|C|S
ARTICLES
Published on Web 03/18/2003

Topochemical Anion Metathesis Routes to the Zr_2N_2S Phases and the Na_2S and ACl Derivatives (A = Na, K, Rb)

C. Stoltz,[†] K. Ramesha,[†] S. A. Sirchio,[†] Z. S. Gönen,[†] B. W. Eichhorn,*[,†] L. Salamanca-Riba,[‡] and J. Gopalakrishnan[§]

Contribution from the Departments of Chemistry and Biochemistry and Materials Engineering, Center for Superconductivity Research, University of Maryland, College Park, Maryland 20742, and Solid State and Structural Chemistry Unit, Indian Institute of Science, Bangalore 560012, India

Received August 8, 2002; E-mail: eichhorn@umd.edu

Abstract: Anion metathesis reactions between ZrNCl and A_2S (A = Na, K, Rb) in the solid state follow three different pathways depending on reaction temperature and reactant stoichiometry: (1) the reaction of ZrNCl with A_2S in the 2:1 stoichiometry at 800 °C/72 h/in vacuo yields α-Zr_2N_2S with the expected layered structure of La_2O_2S. Above 850 °C, α-Zr_2N_2S ($P\bar{3}m1$; $a = 3.605(1)$ Å, $c = 6.421(3)$ Å) neatly transforms to β-Zr_2N_2S ($P6_3/mmc$: $a = 3.602(1)$ Å, $c = 12.817(1)$ Å). The structures of the α- and β-forms are related by an $a/2$ shift of successive Zr_2N_2 layers. (2) The same reaction at low temperatures (300−400 °C) yields ACl intercalated phases of the formula $A_xZr_2N_2SCl_x$ ($0 < x < \sim 0.15$), where alkali ions are inserted between the S/Cl···S/Cl van der Waals gap of a ZrNCl-type structure. The S and Cl ions are disordered and the c lattice parameters are alkali dependent ($R\bar{3}m$, $a \sim 3.6$ Å, $c \sim 28.4$ (Na), 28.9 (K), and 30.5 Å (Rb). $A_xZr_2N_2SCl_x$ phases are hygroscopic and reversibly absorb water to give monohydrates. (3) Reaction of ZrNCl with excess A_2S at 400−1000 °C gives A_2S intercalated phases of the formula $A_{2x}Zr_2N_2S_{1+x}$ ($0 < x < 0.5$), where the alkali ions reside between the S···S van der Waals gap of a ZrNCl type structure ($R\bar{3}m$, $a \sim 3.64$ Å, $c \sim 29.48$ Å). Structural characterization of the new phases and implications of the results are described.

The group 4 nitride−halides have received considerable attention of late due to their interesting structures and physical properties. Recently, it was shown that alkali-doped derivatives of ZrNCl and HfNCl are superconductors with T_c's as high as 25 K.[1−4] The ZrNCl structure is lamellar with a van der Waals-type stacking of Cl−Zr_2N_2−Cl sheets (see I in Chart 1).[5] Various alkali ions and organometallics can be inserted into the van der Waals gap and effectively inject charge into the ZrN layers.[6−10] The superconducting transition temperatures of the intercalated (doped) phases are relatively insensitive to the nature of the intercalant, which is reminiscent of the behavior in the doped A_xMS_2 superconductors (A = alkali, M = early transition metal).[11−13] Unlike the MS_2 derivatives, however, the halide anions of the HfNCl and ZrNCl phases can be changed (Cl → Br → I), which effects a shift to lower T_c in the doped materials.[4,8] For these reasons, we and others have been interested in preparing different derivatives of this class of compounds in order to study the anion effect on T_c and achieve higher transition temperatures.

One intriguing but elusive derivative of this class of materials is the sulfide compound Zr_2N_2S, which is expected[14,15] to have an La_2O_2S structure[16] (see II in Chart 1). The transformation from ZrNCl to Zr_2N_2S involves replacement of two chloride ions by one sulfide ion, which would eliminate the van der Waals gap and covalently link the ZrN layers. Although the synthesis of Zr_2N_2S has not been reported to date, Lissner and Schleid recently described[15] a novel synthetic route to a NaCl-stabilized Zr_2N_2S derivative of formula $NaZr_2N_2SCl$ (see III in Chart 1 and eq 1). The $NaZr_2N_2SCl$ structure is closely related

$$2NaN_3 + 7Zr + 6S + \text{xs NaCl} \rightarrow Na_2ZrS_3 + 3NaZr_2N_2SCl \quad (850\ ^\circ C) \quad (1)$$

to that of ZrNCl. The Na^+ ions of $NaZr_2N_2SCl$ fill the octahedral

[†] Department of Chemistry and Biochemistry, University of Maryland.
[‡] Department of Materials Engineering, University of Maryland.
[§] Indian Institute of Science.

(1) Tou, H.; Maniwa, Y.; Koiwasaki, T.; Yamanaka, S. *Phys. Rev. B* **2001**, *63*, 20508.
(2) Yamanaka, S.; Hotehama, K.; Kawaji, H. *Nature* **1998**, *392*, 580.
(3) Yamanaka, S.; Hotehama, K.; Koiwasaki, T.; Kawaji, H.; Fukuoka, H.; Shamoto, S.; Kajitani, T. *Physica C* **2000**, *341*, 699.
(4) Yamanaka, S.; Kawaji, H.; Hotehama, K.; Ohashi, M. *Adv. Mater.* **1996**, *8*, 771.
(5) Fogg, A. M.; Evans, J. S. O.; O'Hare, D. *Chem. Commun.* **1998**, 2269.
(6) Ohashi, M.; Uyeoka, K.; Yamanaka, S.; Hattori, M. *Chem. Lett.* **1990**, 93.
(7) Ohashi, M.; Uyeoka, K.; Yamanaka, S.; Hattori, M. *Bull. Chem. Soc. Jpn.* **1991**, *64*, 2814.
(8) Kawaji, H.; Hotehama, K.; Yamanaka, S. *Chem. Mater.* **1997**, *9*, 2127.
(9) Fogg, A. M.; Green, V. M.; O'Hare, D. *Chem. Mater.* **1999**, *11*, 216.
(10) Fogg, A. M.; Green, V. M.; O'Hare, D. *J. Mater. Chem.* **1999**, *9*, 1547.
(11) Schöllhorn, R. in *Physics of Intercalation Compounds*; Pietronero, l., Tosatti, E., Eds.; Springer-Verlag: Berlin, New York, 1983; p 33.
(12) *Intercalation Chemistry*; Whittingham, M. S., Jacobson, A. J., Eds.; Academic Press: New York, 1982.
(13) Jacobson, A. J. In *Solid State Chemistry Compounds*; Cheetham, A., Day, P., Eds.; Oxford University Press: New York, 1992; p 182.
(14) Lissner, F.; Schleid, T. *Z. Anorg. Allg. Chem.* **1999**, *625*, 195.
(15) Lissner, F.; Schleid, T. *Z. Anorg. Allg. Chem.* **2001**, *627*, 2307.
(16) Morosin, B. *Acta Crystallogr.* **1973**, *B29*, 2647.

Chart 1

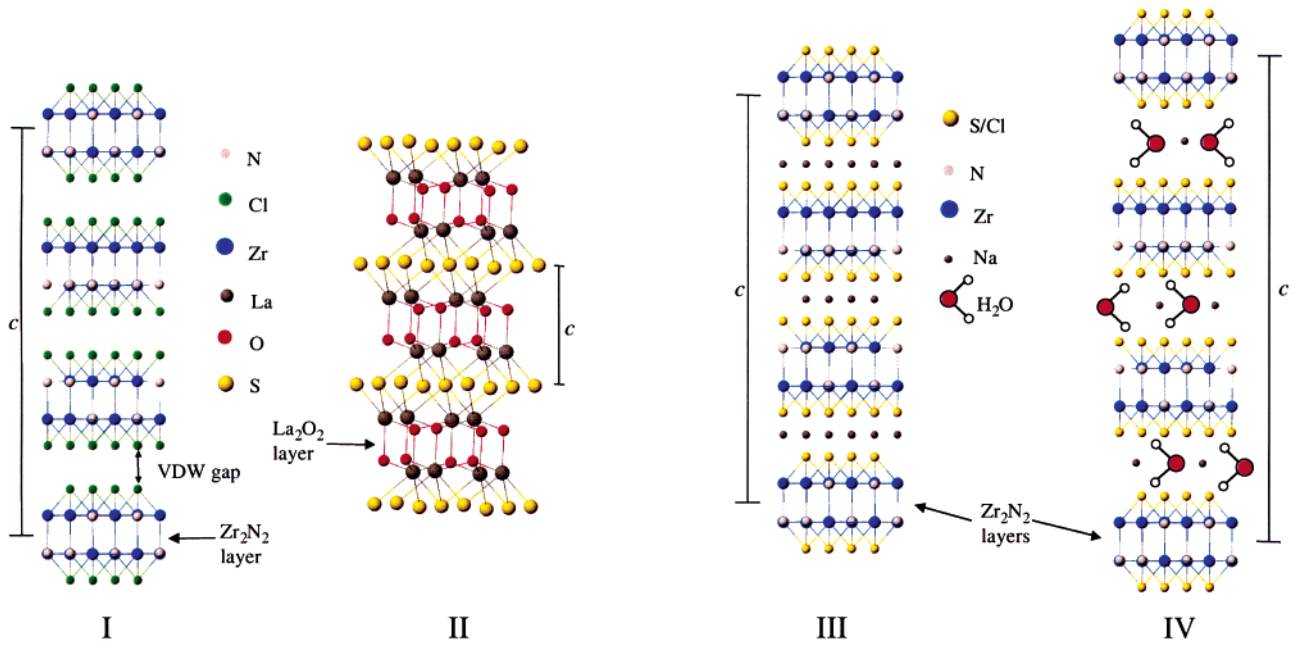

Scheme 1

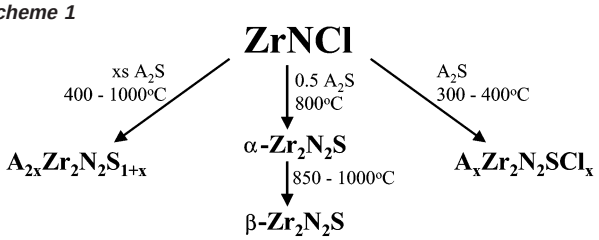

holes in the van der Waals gap of the ZrNCl structure whereas a disordered 1:1 mixture of S and Cl resides on the chloride sites.[15] We report here the synthesis of nonstabilized Zr_2N_2S by way of topotactic anion metathesis chemistry. The low-temperature form of the compound has the expected La_2O_2S structure type ($P\bar{3}m1$ crystal symmetry)[16] but undergoes a phase transition to a more thermodynamically stable β-structure ($P6_3/mmc$ crystal symmetry). In addition, we describe the synthesis and characterization of the Na_2S excess phases, $Na_{2x}Zr_2N_2S_{1+x}$ ($0 < x < 0.5$) and defect members of the Lissner and Schleid-type compounds[15] of formula $A_xZr_2N_2SCl_x$ where A = Na, K, Rb and $0 < x < \sim 0.15$.

Results

Synthesis. ZrNCl reacts with A_2S (A = Na, K, Rb) reagents to give a series of sulfide/chloride materials that depend on reaction conditions and temperature. The reactions are summarized in Scheme 1 and are described individually below.

ZrNCl reacts with $^1/_2$ equiv of A_2S (A = Na, K, Rb) at 800 °C (in vacuo) to give α-Zr_2N_2S and ACl after 72 h according to eq 2. The brown α-Zr_2N_2S product is obtained by removing

$$2ZrNCl + A_2S \rightarrow \alpha\text{-}Zr_2N_2S + 2ACl \quad (A = Na, K, Rb; 800\ °C) \quad (2)$$

the ACl byproduct with water. The compound has been characterized by powder XRD, EDX, TEM, and ED studies. The XRD analysis (Figure 1) shows a ZrO_2 impurity that presumably originates from the ZrNCl starting material. EDX analyses show only Zr and S in a 2:1 ratio after accounting for the ZrO_2 impurity content. The compound has the expected La_2O_2S structure type with $P\bar{3}m1$ crystal symmetry and will be discussed in the next section.

Above 850 °C, α-Zr_2N_2S neatly converts to a different polymorph, β-Zr_2N_2S, that possesses $P6_3/mmc$ crystal symmetry and, to our knowledge, represents a new structure type (see next section). The β-Zr_2N_2S phase can be directly synthesized from the ZrNCl and A_2S precursors when reaction *2* is carried out at 900 °C. The β−phase is dark brownish-green in color and is stable to 1050 °C in the absence of air. This compound has been characterized by EDX, microanalysis, and powder XRD (Rietveld refinement). Both the α- and β-Zr_2N_2S phases are stable in air at room temperature and are not hygroscopic.

Reactions of ZrNCl with excess A_2S (A = Na, K) at 400−1000 °C result in the formation of A_2S excess phases of formula $A_{2x}Zr_2N_2S_{1+x}$ ($0 < x < 0.5$) according to eq 3. The A_2S phases

$$2ZrNCl + 1{+}xA_2S \rightarrow A_{2x}Zr_2N_2S_{1+x} + 2ACl \quad (A = Na, K;\ 400{-}1000\ °C,\ 0 < x < 0.5) \quad (3)$$

appear to exist throughout the range $0 < x \leq 0.5$; however, we have only characterized two members of the series; namely, $Na_{0.5}Zr_2N_2S_{1.25}$ ($x = 0.25$) and $Na_{0.95}Zr_2N_2S_{1.84}$ ($x \approx 0.5$). The Na compounds can be prepared as single-phase materials whereas the potassium compounds $K_{2x}Zr_2N_2S_{1+x}$ are formed competitively with α-Zr_2N_2S and have not been prepared in pure form. Reactions with Rb_2S give exclusively Zr_2N_2S. High synthesis temperatures (~1000 °C) are required to obtain $Na_{2x}Zr_2N_2S_{1+x}$ members with $x > 0.25$. Reactions conducted at 800 °C or below result in a maximum of 25% Na_2S incorporation regardless of reaction stoichiometry. WDS analyses and bulk sulfur microanalyses conducted on the $x = 0.25$ and $x = 0.50$ $Na_{2x}Zr_2N_2S_{1+x}$ compounds gave the formulations (normalized to Zr) of $Na_{0.49(3)}Zr_{2.00(7)}N_2S_{1.28(4)}$ and $Na_{0.90(3)}Zr_{2.0(2)}N_2S_{1.85(1)}$, respectively. The formula are subsequently referred to as $Na_{0.5}Zr_2N_2S_{1.25}$ and $Na_{0.95}Zr_2N_2S_{1.84}$, respectively. The apparent excess sulfur in the $Na_{0.95}Zr_2N_2S_{1.84}$ phase may be due to the presence of disulfide units (S_2^{2-}) within the sulfide

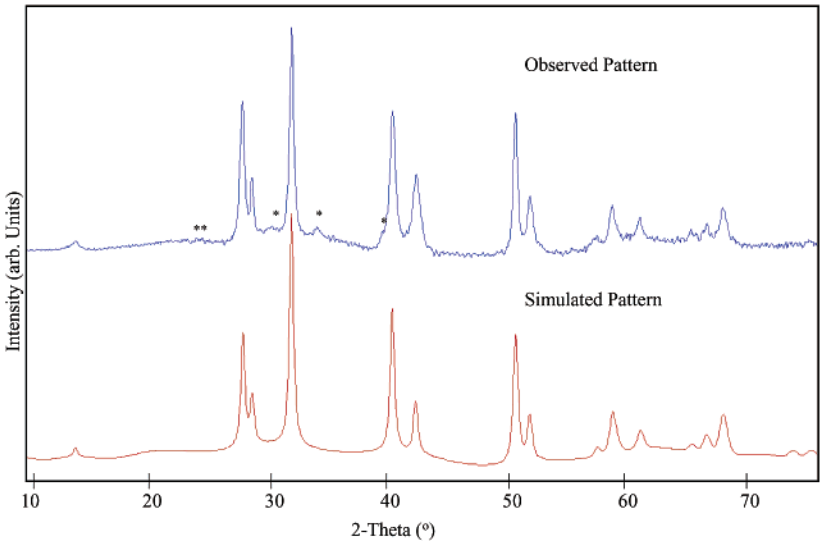

Figure 1. Calculated and observed XRD profiles for α-Zr_2N_2S. The asterisks denote reflections due to the ZrO_2 impurity. The broad background is due to the emerging β-Zr_2N_2S high-temperature phase.

Table 1. Crystallographic Data

empirical formula	$Na_xZr_2N_2SCl_x$[a]	$K_xZr_2N_2SCl_x$[a]	$Rb_xZr_2N_2SCl_x$[a]	$Na_{0.95}Zr_2N_2S_{1.84}$[b]	α-Zr_2N_2S[c]	β-Zr_2N_2S[b]
space group	$R\bar{3}m$	$R\bar{3}m$	$R\bar{3}m$	$R\bar{3}m$	$P\bar{3}m1$	$P6_3/mmc$
a/Å	3.63	3.61	3.57	3.637(1)	3.605(2)	3.611(1)
c/Å	28.4	28.9	30.5	29.490(7)	6.412(3)	12.818(1)
c/Å hydrated	32.5	33.9	33.3			
reaction temp/°C	300−350	300−350	300−350	400−1000	700−800	850−1050

[a] Unit cell estimates from diffraction data. Not refined due to broadness of diffraction peaks. [b] Refined unit cell parameters from Rietveld analysis (Topas, Bruker). [c] Refined unit cell from diffracction data (MDI; Jade).

layer. The $A_{2x}Zr_2N_2S_{1+x}$ compounds adopt a highly defective $NaZr_2N_2SCl$ type structure (see III in Chart 1). The compounds are yellow-brown in color, free of chloride (WDS and EDX analyses), and stable in air at room temperature.

The sulfide-for-chloride exchange also occurs at much lower temperatures (300−400 °C), but the resulting products contain residual alkali halide (5−15 mol %) and adopt a highly defective $NaZr_2N_2SCl$-type structure (see III in Chart 1 and eq 4). The

$$2ZrNCl + A_2S \rightarrow A_xZr_2N_2SCl_x + 2-xACl \quad (A = Na, K;\ 0 < x \leq 0.15;\ 300-400\ °C) \quad (4)$$

use of excess Na_2S in the reactions or regrinding and refiring with additional Na_2S does not reduce the amount of residual chloride in the 300−350 °C temperature regime. Although the product compositions vary with reaction temperature, conditions, and time, the general formula for these compounds is given by $Na_xZr_2N_2SCl_x$, where $0 < x \leq \sim 0.15$ (see below).

The $x = 1$ end member is the $NaZr_2N_2SCl$ phase described by Lissner and Schleid[15] but cannot be prepared by this chemistry. Due to the low reaction temperatures, the compounds are poorly crystalline (see next section) but the prominent 0 0 3 reflections show that the *c* lattice parameter increases with the size of the alkali ion (see Table 1).

Unlike the Zr_2N_2S and $A_{2x}Zr_2N_2S_{1+x}$ phases, the $A_xZr_2N_2SCl_x$ compounds are hygroscopic and reversibly form monohydrates of formula $A_x(H_2O)Zr_2N_2SCl_x$ (see eq 5). The *c* lattice

$$A_xZr_2N_2SCl_x + H_2O \rightleftarrows A_x(H_2O)Zr_2N_2SCl_x \quad (5)$$

parameters of the hydrated materials (~33−34 Å; see next section) are relatively insensitive to the size of the alkali ions and are presumably dictated by the size of the H_2O intercalant (see IV in Chart 1). TGA analyses indicate that approximately one water molecule of hydration is incorporated for each Zr_2N_2S subunit. The exact hydration level is difficult to determine due to the heterogeneity of the sample (see below). The alkali chloride-stabilized compounds have been characterized by powder XRD, EDX, WDS, TEM, and ED analysis. The WDS/EDX analyses from stoichiometric reactions are highly variable from sample to sample showing 5−15% ACl contents, but Cl is often in significantly higher concentration than the alkali content. The data indicate that the products are most likely heterogeneous with various members of the $A_xZr_2N_2SCl_x$ solid solution, the corresponding hydrates, and potentially some products from incomplete metathesis.

Structural Studies. A summary of the structural data is given in Table 1. Each compound is described individually below.

α-Zr_2N_2S. The low-temperature α-Zr_2N_2S compound adopts the expected[14,15] La_2O_2S structure[16] with $P\bar{3}m1$ crystal symmetry where $a = 3.605(1)$ Å and $c = 6.412(3)$ Å. The crystal symmetry has been assigned on the basis of the XRD patterns, the TEM data, and the electron diffraction studies. The simulated and observed XRD profiles are shown in Figure 1, and an idealized ball-and-stick drawing of the structure is given in Figure 2. The broad background in the diffraction profile arises from the emerging β-Zr_2N_2S phase (see next section) that crystallizes above 850 °C. The ZrO_2 impurity presumably originates from the ZrNCl starting material. Regardless, the agreement between calculated and observed XRD profiles is excellent.

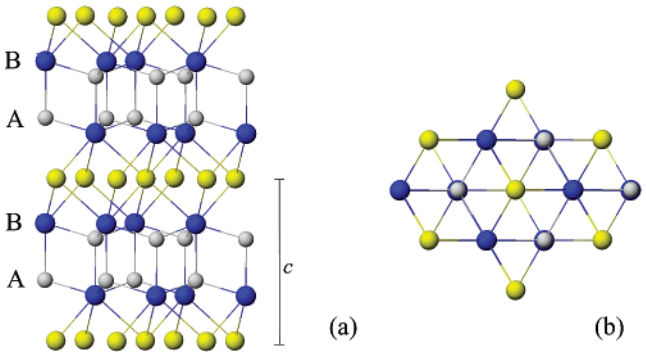

Figure 2. Idealized ball-and-stick drawing of the α-Zr_2N_2S structure (a) perpendicular to the *c*-axis and (b) down the *c*-axis. The coloring scheme is as follows: zirconium, blue; sulfur, yellow; nitrogen, light gray.

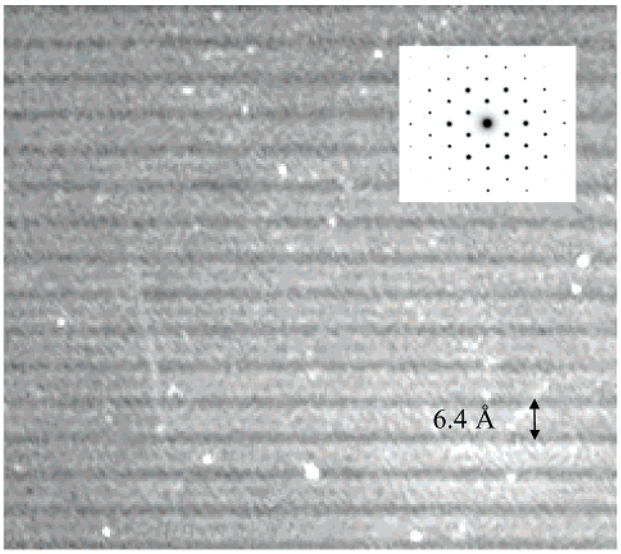

Figure 3. TEM image of the α-Zr_2N_2S showing the [1 0 0] zone axis and the 6.4 Å unit cell. The inset shows the electron diffraction pattern, which is consistent with the La_2O_2S structure type.

The TEM image of α-Zr_2N_2S (Figure 3) shows the layered nature of the structure and the well-defined 6.4 Å repeat unit that defines the *c* lattice parameter. The selected area electron diffraction (SAED) studies of the [0 0 1] zone axis (see inset, Figure 3) are also consistent with the refined unit cell parameters and crystal symmetry and do not reveal any superstructure reflections.

The α-Zr_2N_2S structure contains Zr_2N_2 layers similar to that of *β*-ZrNCl and related zirconium nitrides. The individual ZrN layers stack in an AB···AB···AB repeat pattern that gives rise to interlayer Zr_6 octahedral holes and the 6.4-Å *c* lattice parameter (Figure 3). Due to the broadness of the diffraction profiles and the emergence of the *β*-Zr_2N_2S phase, we could not obtain reasonable refinements of the structure. However, the idealized model constructed from the refined unit cell constants imposed on the La_2O_2S structure type gives very reasonable metric parameters. In the idealized model, each Zr is 7 coordinate with a ZrN_4S_3 coordination sphere (see Figure 4a). When the Zr−N distances are adjusted to equal those of *β*-ZrNCl, the optimized Zr−S distances are 2.74 Å. For comparison, the Zr−S distances in $NaZr_2S_3$ and the $Ba_{n+1}Zr_nS_{3n+1}$ perovskites are 2.5−2.6 Å (av)[14,17,18] but the sulfur and zirconium coordination numbers are lower in the later compounds. The sulfur atoms of α-Zr_2N_2S symmetrically bridge the ZrN layers and reside in Zr_6 octahedral holes (see Figure 4b).

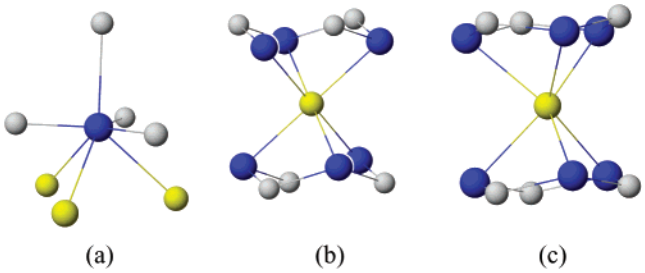

Figure 4. Ball-and-stick drawing of (a) the ZrN_4S_3 coordination sphere of Zr_2N_2S compounds, (b) the octahedral SZr_6 site in α-Zr_2N_2S, and (c) the trigonal prismatic SZr_6 site in *β*-Zr_2N_2S. The coloring scheme is as follows: zirconium, blue; sulfur, yellow; nitrogen, light gray.

***β*-Zr_2N_2S.** The high-temperature form of Zr_2N_2S, denoted *β*-Zr_2N_2S, adopts a new structure type with $P6_3/mmc$ crystal symmetry with $a = 3.611(1)$ Å and $c = 12.818(1)$ Å. The calculated, observed, and difference XRD profiles for *β*-Zr_2N_2S are shown in Figure 5 and a ball-and-stick drawing of this structure is given in Figure 6. A summary of the refinement data is given in Table 2 and selected bond distances and angles are given in Table 3. The ZrO_2 impurity in the sample was accommodated by way of a two-phase refinement. The *β*-Zr_2N_2S structure differs from the α-form by shifting the interleaving Zr_2N_2 layers by *a*/2, which leaves the interlayer sulfide ions in trigonal prismatic Zr_6 holes instead of octahedral holes (see Figure 4c). The shift changes the stacking of the ZrN layers along the *c* axis to give an AB···BA···AB··· repeat sequence (Figure 6). This alternate stacking sequence doubles the *c* lattice parameter relative to the AB···AB···AB arrangement in the α-structure and generates the trigonal prismatic Zr_6 interlayer holes. The shift also aligns the Zr atoms from adjacent layers along the *c* axis. However, the zirconium coordination sphere and individual ZrN layers are the same in both forms. The refined Zr−S distances (2.814(1) Å) are again long relative to other zirconium sulfides[14,17,18] and presumably reflect the high coordination numbers (CNs) of both sulfur (CN = 6) and zirconium (CN = 7). The refined Zr−N distances (2.10, 2.35 Å) are quite reasonable[15] but are less reliable due to the low scattering power of nitrogen.

$Na_{2x}Zr_2N_2S_{1+x}$. The structure of the $Na_{2x}Zr_2N_2S_{1+x}$ phases is closely related to that of *β*-ZrNCl and $NaZr_2N_2SCl$. The compounds are rhombohedral, space group $R\bar{3}m$, with $a \approx 3.6$ Å and $c \approx 29.5$ Å. The results of a Rietveld refinement for $Na_{0.95}Zr_2N_2S_{1.84}$ are given in Table 2, and selected bond distances and angles are given in Table 3. The calculated, observed, and difference XRD profiles are shown in Figure 7. The analytical data gave a formula of $Na_{0.90(3)}Zr_{2.0(2)}N_2S_{1.85(1)}$, which is in excellent agreement with the refined occupancies of $Na_{0.95(2)}Zr_2N_2S_{1.84(3)}$ for the same sample. The structure is essentially that of $NaZr_2N_2SCl$ (see III in Chart 1) with the following exceptions. The excess sulfide in the $Na_{0.95}Zr_2N_2S_{1.84}$ formula (i.e. for $x = 0.47$ in $Na_{2x}Zr_2N_2S_{1+x}$; Na = 0.95 and S = 1.47) presumably arises from the formation of disulfide units in the sulfide layer. The formation of disulfides is quite common

(17) Chen, B.-H.; Eichhorn, B.; Fanwick, P. *Inorg. Chem.* **1992**, *31*, 1788.

(18) Hung, Y.-C.; Fettinger, J. C.; Eichhorn, B. W. *Acta Crystallogr.* **1997**, *C53*, 827.

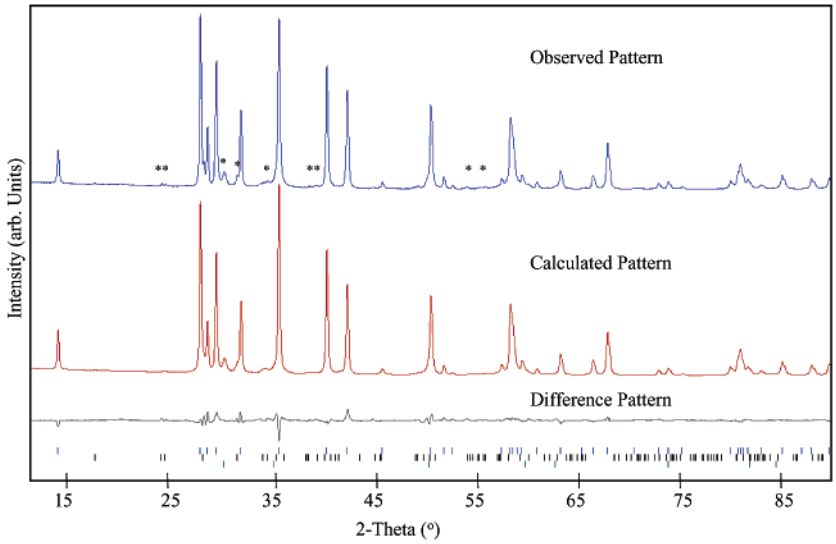

Figure 5. Calculated, observed, and difference XRD profiles (Rietveld analysis, Topas) for β-Zr_2N_2S. The asterisks denote the ZrO_2 impurities (two polymorphs) that were accommodated by way of a three-phase refinement. The tick marks indicate the Bragg reflections for β-Zr_2N_2S (top), ZrO_2 JCPDF 83-0939 (middle), and ZrO_2 JCPDF 81-1550 (bottom).

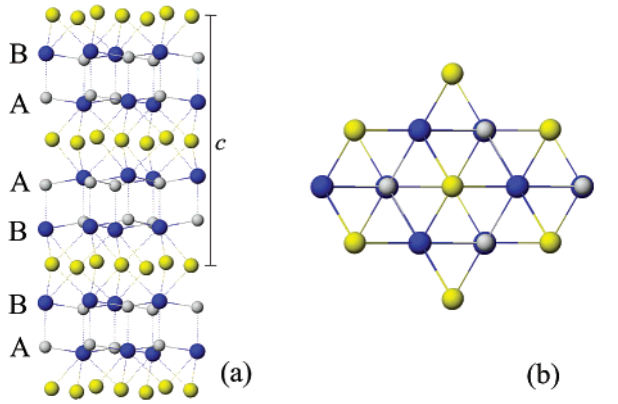

Figure 6. Ball-and-stick drawing of the β-Zr_2N_2S structure showing (a) an approximate 1 0 0 projection and (b) a 0 0 1 projection. The coloring scheme is as follows: zirconium, blue; sulfur, yellow; nitrogen, light gray.

and would alleviate instabilities associated with large vacancy concentrations. However, in $Na_{0.95}Zr_2N_2S_{1.84}$, the sulfide layer still contains ~15% vacancies that are randomly distributed. For lower x members in the $Na_{2x}Zr_2N_2S_{1+x}$ series, the vacancies approach 50%. Although we do not detect disulfides in these compounds through composition analysis, it is quite possible that disulfide units could exist there as well.

The octahedral sites that host the Na^+ ions in the van der Waals gaps can be fully occupied ($x = 0.5$) or virtually empty as x approaches zero. This behavior is quite similar to that of the A_xMS_2 compounds (A = alkali, M = early transition metal),[11−13] where x can vary from 0 to 1. The unit cell parameters for $Na_{0.5}Zr_2N_2S_{1.25}$ ($a = 3.634(1)$ Å, $c = 29.469(7)$ Å) are very similar to those of $Na_{0.95}Zr_2N_2S_{1.84}$ ($a = 3.637(1)$ Å, $c = 29.490(7)$ Å).

The Zr−S bond distances for $NaZr_2N_2S_{1.5}$ are 2.671(2) Å, which are shorter than those of the Zr_2N_2S phases and are more akin to other zirconium sulfides.[14,17,18] The shorter distances presumably reflect the lower coordination numbers of both Zr and S due to vacancies in the $NaZr_2N_2S_{1.5}$ structure. The refined Zr−N and Na−S distances are typical.[5,15]

$A_xZr_2N_2SCl_x$ and Its Hydrates. The $A_xZr_2N_2SCl_x$ phases are also isostructural with the Lissner and Schleid compound

Table 2. XRD Rietveld Refinement Data

		β-Zr_2N_2S	$Na_{0.95}Zr_2N_2S_{1.84}$
crystal system		hexagonal	trigonal
space group		$P6_3/mmc$	$R\bar{3}m$
a/Å		3.611(1)	3.637(1)
c/Å		12.818(1)	29.490(7)
Pref Or		0 0 1	0 0 1
R_{wp}		7.8	9.5
R_p		5.9	6.11
R_{Bragg}		4.1	4.1
Zr	x	1/3	0
	y	2/3	0
	z	0.8975(1)	0.2135(3)
	Beq	0.21(8)	0.46(6)
	occ	1.0	1.0
N	x	1/3	0
	y	2/3	0
	z	0.0809(5)	0.1430(3)
	Beq	0.10	0.20
	occ	1.0	1.0
S	x	0	0
	y	0	0
	z	1/4	0.3973(1)
	Beq	0.10(1)	0.08(1)
	occ	1.0	0.918(5)
Na	x		0
	y		0
	z		0
	Beq		2.0(2)
	occ		0.95(2)

$NaZr_2N_2SCl$ (see III in Chart 1)[15] but have vacancies on both the Na and S/Cl sites. The compounds are rhombohedral, space group $R\bar{3}m$, with alkali-dependent lattice parameters of $a \approx 3.6$ Å and $c = 28.4$ (Na), 28.9 (K), and 30.5 Å (Rb). The crystal symmetries and structures are based upon the similarities with the well-characterized[15] $NaZr_2N_2SCl$ end member, the XRD profiles, and the TEM and ED data. Because layer shifts and alternate crystal symmetries are well known for layered oxides with large alkali ions,[19] the actual crystal symmetry for the Rb phase may be different. The XRD profiles are characteristically broad in appearance (see Figure 8) and are quite similar to those of ZrNCl as expected. The c lattice constants were estimated

(19) Schaak, R. E.; Mallouk, T. E. *Chem. Mater.* **2002**, *14*, 1455.

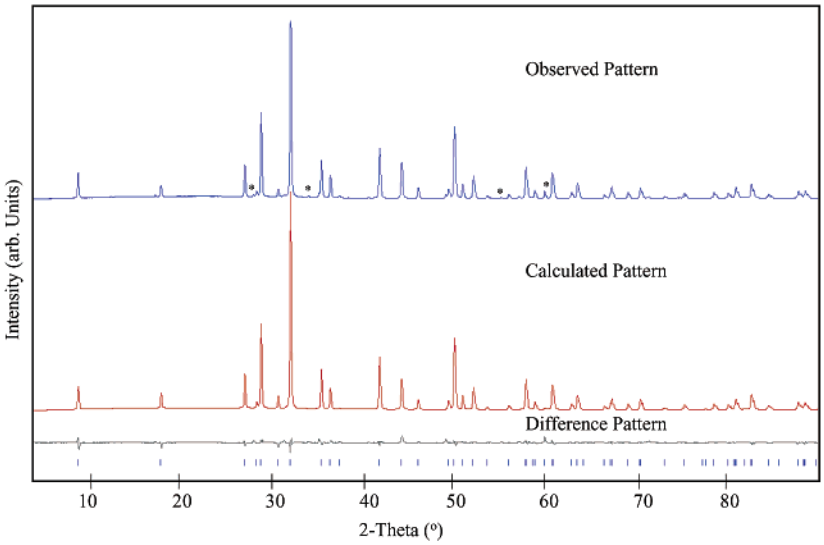

Figure 7. Calculated, observed, and difference XRD profiles (Rietveld analysis, Topas) for $Na_{0.95}Zr_2N_2S_{1.84}$. The asterisks denote the ZrO_2 impurities (not refined). The tick marks indicate the $Na_{0.95}Zr_2N_2S_{1.84}$ Bragg reflections.

Table 3. Selected Bond Distances (Å) and Angles (deg)

	β-Zr_2N_2S	$Na_{0.95}Zr_2N_2S_{1.84}$
Zr−N	2.103(1)	2.078(12)
Zr−N	2.35(1)	2.208(4)
Zr−S	2.814(1)	2.671(2)
Na−S		2.822(2)
N−Zr−N	118.3(2)	110.9(3)
N−Zr−N	82.4(2)	72.0(3)
Zr−N−Zr	97.6(2)	108.0(3)
Zr−S−Zr	82.4(2)	85.8(1)
S−Zr−S	79.81(1)	
S−Na−S		99.7(1)
S−Na−S		80.3(1)

from the 0 0 3 reflections and the TEM images whereas the *a* lattice constants were estimated from the electron diffraction data and the higher angle diffraction data. Cell constants and structures could not be refined due to the low quality of the diffraction data.

The hydrated samples contain water molecules in the intergallery sites, and all of the $A_xZr_2N_2SCl_x(H_2O)$ phases (where A = Na, K, Rb) have *c* lattice parameters of ∼33−34 Å (see IV in Chart 1 and Table 1). The TEM images of the dehydrated (Figure 9a) and hydrated (Figure 9b) potassium phase shows the 29- and 34-Å lattice spacings, respectively, in accord with the observed XRD profiles (see Figure 8). Importantly, the TEM images of the hydrated phase show both hydrated and dehydrated regions in the same crystallite (see Figure 9b), which is consistent with the reversible nature of the hydration process (eq 5). The insensitivity of the *c* parameters to the size of the alkali ion in the hydrated samples indicates that the intergallery spacing is dominated by water molecules that are presumably H-bonded to the Cl/S anions (see IV in Chart 1). The exact crystal symmetries of the hydrated phases are unkown.

Discussion

Cation methathesis in layered oxides has received significant recent attention as a method of preparing low-temperature and metastable-layered oxides.[19−21] By exploiting the hydrophobic/

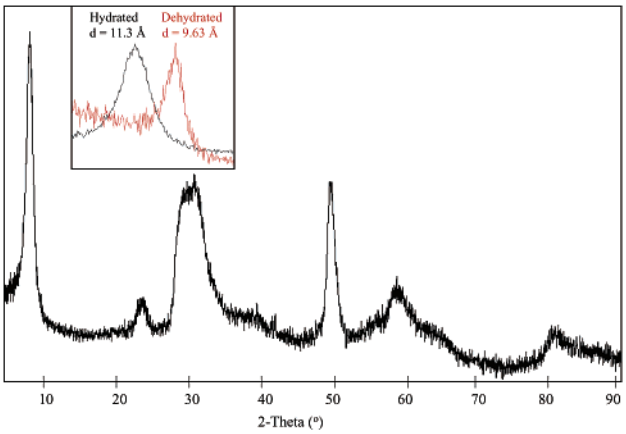

Figure 8. XRD profile for $K_xZr_2N_2SCl_x(H_2O)$, where $x \sim 0.15$. The inset shows the 0 0 3 peak shift upon hydration.

hydrophilic interactions of organic and inorganic layers, one can obtain exfoliated monolayers and nanotubes by inserting organic cations between the layers of inorganic oxides.[22,23] However, the intergallery exchangeable cations in layered oxides are highly ionic by design and have little electronic or chemical influence on the host oxide matrix. In contrast, since anions are an integral part of the host, exchange of anions in layered materials can directly alter the band structure of the host lattice. Moreover, if organic anions can be incorporated into the host, they can directly affect the electronic properties of the materials through covalent interactions and potentially introduce additional functionality. Of course, topotactic anion exchange is much more difficult than cation exchange due to the anion's large size and high polarizability. However, the sulfide-for-chloride exchanges described here illustrate that such transformations are indeed possible and also give rise to new solid-state compounds that are not accessible by traditional means. Importantly, these reactions illustrate that generic coordination chemistry available

(20) Sivakumar, T.; Seshadri, R.; Gopalakrishnan, J. *J. Am. Chem. Soc.* **2001**, *123*, 11496.
(21) Gopalakrishnan, J.; Sivakumar, T.; Ramesha, K.; Thangadurai, V.; Subbanna, G. N. *J. Am. Chem. Soc.* **2000**, *122*, 6237.
(22) Urban, J. J.; Yun, W. S.; Gu, Q.; Park, H., *J. Am. Chem. Soc.* **2002**, *124*, 1186.
(23) Schaak, R. E.; Mallouk, T. E. *Chem. Mater.* **2000**, *12*, 3427.

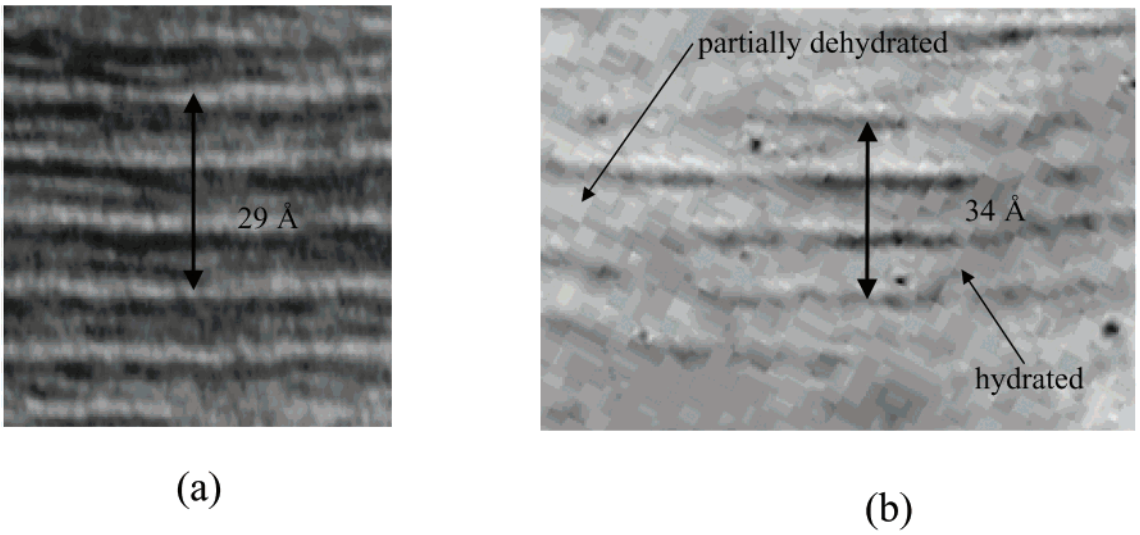

Figure 9. TEM image of $K_xZr_2N_2SCl_x$, where $x \sim 0.15$. (a) A crystallite showing a dehydrated $K_xZr_2N_2SCl_x$ region; (b) a crystallite showing dehydrated and hydrated $K_xZr_2N_2SCl_x$ regions.

to the molecular chemist may be viable in these and related layered halides.

Ironically, the poor crystallinity and small particle size of the ZrNCl precursor, which makes characterization difficult, is presumably a key feature in the success of the metathesis chemistry described here. Highly crystalline ZrNCl starting materials show much slower reaction kinetics for metathesis, which is consistent with a topochemical metathesis exchange process.

The sulfide-for-chloride exchange reactions described here show that kinetic control can be obtained in a topchemical anion exchange process involving a refractory inorganic host matrix. To our knowledge, there are no alternate synthetic routes to either form of Zr_2N_2S, and in addition, the reduced temperatures associated with the metathesis routes allow for the isolation of the low-temperature α-Zr_2N_2S form. Conversion to the β-form is irreversible. It is also interesting to note that the Zr_2N_2S phases are formed competitively with the $Na_{2x}Zr_2N_2S_{1+x}$ compound and cannot be interconverted. For example, neither phase of Zr_2N_2S reacts with Na_2S or NaCl to form the respective $Na_{2x}Zr_2N_2S_{1+x}$ or $Na_xZr_2N_2SCl_x$ compounds. Likewise, the $Na_{2x}Zr_2N_2S_{1+x}$ phases do not undergo deintercalation reactions to form Zr_2N_2S at any temperature. In contrast, the anhydrous $Na_xZr_2N_2SCl_x$ compounds are intermediates in the formation of the Zr_2N_2S phases. The synthesis of the Zr_2N_2S phases are favored at high temperatures (>650 °C), and even though NaCl is a byproduct of the reaction (see eq 2), the NaCl intercalation products are not obtained under the high-temperature conditions described herein. This observation suggests that these topochemical reactions are quite different from that involving the direct synthesis of $NaZr_2N_2SCl$ described by Lissner and Schleid (see eq 1). The latter was prepared at a similar reaction temperature (800 °C) but does not afford the desired Zr_2N_2S phases. Moreover, our low-temperature chemistry gives low x members of the $Na_xZr_2N_2SCl_x$ phases but does not give the Lissner and Schleid end member $NaZr_2N_2SCl$.[15] These data show that topochemical exchange chemistry described here is mechanistically distinct and gives rise to different products.

Conlclusion

We have shown that anion exchange reactions between ZrNCl and A_2S (A = Na, K, Rb) in the solid state follow three different pathways depending on reaction temperature and reactant stoichiometry. The reactions of ZrNCl with A_2S in the 2:1 stoichiometry gives α-Zr_2N_2S with the expected layered structure of La_2O_2S at 800 °C but gives β-Zr_2N_2S above 850 °C. The structures of the α- and β-forms are related by an $a/2$ shift of successive Zr_2N_2 layers. The same reaction at low temperatures (300−400 °C) yields ACl intercalated phases of the formula $A_xZr_2N_2SCl_x$ ($0 < x < \sim 0.2$) that are defect derivatives of the Lissner and Schlied compound $NaZr_2N_2SCl$.[15] Reactions of ZrNCl with excess A_2S at 400−1000 °C give A_2S intercalated phases of the formula $A_{2x}Zr_2N_2S_{1+x}$ ($0 < x < 0.5$), where the alkali ions reside between the S···S van der Waals gap of a ZrNCl-type structure. Importantly, these anion methathesis synthetic procedures appear to be the only routes to the new materials described here and may evolve into a general method for the preparation of a wide variety of new, fuctionalized compounds.

Experimental Section

General Information. Air- and moisture-sensitive materials were stored and handled in a nitrogen-filled Vacuum Atmospheres drybox. Standard Schlenk techniques were used for all air-sensitive solution processes. Microanalysis was performed by Atlantic Microlab, Inc. (Norcross, GA).

Synthesis. β-ZrNCl was prepared using slight modifications of previously reported methods.[24] In a typical reaction, 1.5 g of Zr metal (99.7% Cerac, 325 mesh) was placed in a quartz boat in the center of an argon flow-through furnace. Approximately 12 g of dry, sublimed NH_4Cl was placed in a second quartz boat ~12 cm from the center of the furnace in the direction of the argon inlet. The furnace was purged with argon for 10 h and then heated at 30 °C/min to 650 °C. The ammonium chloride was heated to ~350 °C, while the boat containing the Zr metal at the center of the furnace was heated to 650 °C, as determined by external thermocouple readings. After cooling to room temperature under argon, the center boat containing amorphous β-ZrNCl

(24) Ohashi, M.; Yamanaka, S.; Sumihara, M.; Hattori, M. *J. Solid State Chem.* **1988**, *75*, 99.

was removed. Occasionally, a thin layer of white ZrO_2 forms on the surface of the product that is manually scraped away to give the pale green product.

A_2S (A = Na, K, Rb) reagents were prepared by direct, stoichiometric reactions of the alkali metals with sulfur in refluxing liquid ammonia. The resulting products were stored in the drybox. **Caution:** reactions using liquid ammonia should be properly cooled and vented to avoid dangerous pressure buildup and explosion.

α-Zr_2N_2S and β-Zr_2N_2S were prepared by the following methods. In a typical reaction, 91 mg (1.0 mmol) of ZrNCl and 39 mg (0.5 mmol) of Na_2S or 55 mg (0.5 mmol) of K_2S were ground and intimately mixed. The mixtures were loaded into silica tubes in the drybox and subsequently evacuated and sealed. During evacuation, a heat gun was used to warm the reaction mixtures to ~200 °C in order to drive off any residual moisture. α-Zr_2N_2S was prepared by heating the samples at 1 °C/min to 800 °C for 3 days. β-Zr_2N_2S was prepared by heating 1 °C/min to 900 °C for 3 days. α-Zr_2N_2S is brown whereas β-Zr_2N_2S is dark brownish-green in color.

$A_{2x}Zr_2N_2S_{1+x}$ was prepared according to the above procedure, using appropriate stoichiometric amounts of ZrNCl and Na_2S, and heating to 800−1000 °C for 3 days. The title compounds are yellow-brown in color. A less crystalline product is obtained between 400 and 800 °C.

$A_xZr_2N_2SCl_x$ was also prepared by a similar procedure. In a typical reaction, 91 mg (1.0 mmol) of ZrNCl and 39 mg (0.5 mmol) of Na_2S were heated to 350 °C for 7 days yielding a tan product. In all reactions, excess alkali halide salt byproducts were washed away by sonicating with 10 mL of distilled water 4 times, followed by a final acetone wash. For the $A_xZr_2N_2SCl_x$ compounds, washing, exposure to air, or both resulted in the formation of the hydrated $A_xZr_2N_2SCl_x(H_2O)$ phases. The hydrates are quantitatively converted back to the anhydrous form by heating the samples under dynamic vacuum at 200 °C. XRD data for the anhydrous material were recorded using sealed, anaerobic sample holders.

Characterization. X-ray diffraction (XRD) patterns were recorded using a Bruker C2 Discover X-ray powder diffractometer with an HiStar area detector and Cu Kα radiation. Typically, five frames were collected and merged to give 2θ scans from 4° to 93°. Unit cell indexing and Rietveld refinements were performed using MDI Jade[25] and Topas[26] software packages, respectively. Parameters in the refinements were introduced in a stepwise fashion. With the exception of the thermal parameters and occupancies, all parameters were refined together in the latter stages. In the final stages, the thermal parameters or occupancies were refined in alternate cycles, with all other parameters fixed, until convergence was reached. For both refinements, the nitrogen thermal parameters and occupancies were fixed at idealized values. Because of the layered nature of the structures, preferred orientations were included. The simulation of α-Zr_2N_2S was performed using Topas software with the La_2O_2S fractional coordinates[16] and the refined cell constants of α-Zr_2N_2S. The background peak profiles were refined to better simulate the observed diffractograms. The coordinates and thermal parameters were fixed at ideal values and not refined.

Energy dispersive X-ray analysis (EDX) was performed with an AMRAY 1820K scanning electron microscope with an acceleration potential of 20 kV. Wavelength dispersive spectroscopy (WDS) was performed with the JXA-8900 Superprobe, using ZrNCl as a Zr and Cl standard, molybdenite as a S standard, albite as a Na standard, and $K_2La_2Ti_3O_{10}$ as a K standard. Samples and standards were mounted into casting resin epoxy plugs. EDX and WDS measurements were carried out by analyzing 10 spots/sample.

Compound formulas were calculated from WDS data and microanalysis data. The nitrogen contents were assumed to be 2.0. The reported errors were generated from propagated counting statistics associated with the WDS analysis.

Hydration-TGA analysis was carried out in a series of three runs by heating the sample in a small Pt boat at 200 °C, starting with initial product masses of ~300 mg.

High-resolution transmission electron micrographs were recorded using a JEOL 4000 FX transmission electron microscope operated at 300 kV. A 200-mesh copper grid with a Formvar/carbon film was introduced in the vial containing the powder of the sample to get some of the nanoparticles attached to the film. Electron diffraction patterns and high-resolution lattice images were obtained from several nanoparticles to get statistical information on the structure of the powder.

Acknowledgment. We are grateful to the NSF-DMR for support of this work and the LINK foundation for the fellowship for Z.S.G.

JA0210650

(25) Jade 5.0, general profile analysis software for powder diffraction data. Materials Data, Inc., Livermore, CA, 1999.
(26) Topas v.2.0, general profile and structure analysis software for powder diffraction data. Bruker AXS, Karlsruhe, Germany, 2000.